Journal of ELECTRONIC MATERIALS, Vol. 42, No. 7, 2013
DOI: 10.1007/s11664-012-2241-0

Fabrication and Evaluation of a Skutterudite-Based Thermoelectric Module for High-Temperature Applications

JORGE GARCÍA-CAÑADAS,[1,4] ANTHONY V. POWELL,[2] ANDREAS KALTZOGLOU,[2] PAZ VAQUEIRO,[2] and GAO MIN[1,3]

1.—Cardiff School of Engineering, Cardiff University, The Parade, Cardiff CF24 3AA, UK. 2.—Department of Chemistry & Centre for Advanced Energy Storage and Recovery, Heriot-Watt University, Edinburgh EH14 4AS, UK. 3.—e-mail: min@cardiff.ac.uk. 4.—e-mail: garciacanadasj@cardiff.ac.uk

We report a straightforward methodology for the fabrication of high-temperature thermoelectric (TE) modules using commercially available solder alloys and metal barriers. This methodology employs standard and accessible facilities that are simple to implement in any laboratory. A TE module formed by nine *n*-type $Yb_xCo_4Sb_{12}$ and *p*-type $Ce_xFe_3CoSb_{12}$ state-of-the-art skutterudite material couples was fabricated. The physical properties of the synthesized skutterudites were determined, and the module power output, internal resistance, and thermocycling stability were evaluated in air. At a temperature difference of 365 K, the module provides more than 1.5 W cm^{-3} volume power density. However, thermocycling showed an increase of the internal module resistance and degradation in performance with the number of cycles when the device is operated at a hot-side temperature higher than 573 K. This may be attributed to oxidation of the skutterudite thermoelements.

Key words: Thermoelectric generator, skutterudites, manufacturing, electrical contact resistivity, power output, device fabrication

INTRODUCTION

Thermoelectric (TE) devices have been identified as promising converters for energy harvesting due to their capability to convert heat into electricity.[1] A great amount of heat is released from high -temperature systems such as internal combustion engines, industrial furnaces, and incinerators. A wide range of materials able to work at different temperature ranges have recently appeared showing relatively high efficiencies, given by the TE figure of merit *ZT*.[2] However, there are significant parasitic losses when the materials are integrated to form a complete device, which lower the device efficiency below the value predicted on the basis of the *ZT* of the component materials. Reduction of these losses is a key challenge to achieve efficient TE devices.[3] This requires the creation of contacts with suitable electrical and thermal properties. When the device operates under a large temperature difference, thermomechanical stress, diffusion, and chemical reaction of materials at the interfaces become important concerns. As TE materials have high electrical conductivities, very low electrical contact resistances are required between the materials and the electrodes, which themselves should have high electrical and thermal conductivities relative to the TE materials. Additionally, the electrodes often include diffusion barriers to prevent diffusion of certain electrode materials into the thermoelements and vice versa, because such diffusion can produce poisoning and degradation of the materials. Moreover, commercial solder alloys with melting points in the 573 K to 973 K range are difficult to find,[4] and sometimes suitable joining materials have to be synthesized[5,6] or the contacts prepared by using additional techniques such as spark plasma sintering[7,8] or hot-pressing,[9] complicating the manufacturing processes. Herein, we present a simple methodology for the fabrication of high-temperature TE devices. It is based on the use

(Received July 7, 2012; accepted August 9, 2012; published online September 6, 2012)

of standard facilities such as a tube furnace and commercially available materials (solders, fluxes, metal barriers, and ceramic plates). To prove the feasibility of the methodology, a skutterudite-based module was fabricated with state-of-the-art materials. The low cost and good performance of skutterudites at high temperatures make them some of the most promising materials for waste heat recovery in this temperature range.[10] The power generation of the fabricated module and its stability under thermocycling are evaluated.

EXPERIMENTAL PROCEDURES

Materials Synthesis and Characterization

The *n*-type $Yb_{0.36}Co_4Sb_{12}$ and *p*-type $Ce_{0.8}Fe_3CoSb_{12}$ skutterudites were synthesized by mixing stoichiometric quantities of the elements Ce (Aldrich, 99.9%), Yb (Aldrich, 99.9%), Fe (Alfa, 99.9%), Co (Aldrich, 99.995%), and Sb (Aldrich, 99.999%) in an argon-filled glove box. The reaction mixtures were loaded into glassy carbon crucibles, which were placed in fused silica tubes. The tubes were transferred to a vacuum line, evacuated ($<10^{-4}$ torr), and sealed. $Yb_{0.36}Co_4Sb_{12}$ was prepared by heating at 1073 K for 1 day before annealing at 873 K for 3 days. $Ce_{0.8}Fe_3CoSb_{12}$ was heated at 1273 K for 12 h, followed by quenching in water and annealing at 873 K for 4 days. The polycrystalline products were characterized using a Bruker D8 Advance powder diffractometer, operating with Ge-monochromated Cu $K_{\alpha 1}$ radiation (λ = 1.5406 Å) and a LynxEye linear detector. Data were collected over the 2θ angular range from 10° to 120° at steps of 0.0092° in detector position. Rietveld refinements were performed with the GSAS software package.[11]

The synthesized materials were finely ground in an agate mortar and loaded into graphite dies and hot-pressed at 900 K (60 MPa, 30 min) under a N_2 atmosphere. The densities of the pellets reached ca. 95% of crystallographic values. Rectangular blocks with approximate dimensions of 2 mm × 2 mm × 10 mm were cut from the pellets with a low-speed diamond saw (MTI Corporation, SYJ-150) and polished with fine sandpaper. Electrical resistivity and Seebeck coefficient measurements were performed simultaneously on a Linseis LSR-3 instrument over the temperature range from 310 K to 610 K under a static He atmosphere (pressure 1.1 bar to 1.4 bar). Data were collected with 1 min waiting time at each point. The sample was mounted on Pt electrodes, and two thermocouple probes were attached on one side. Electrical resistivity was measured with the four-point direct-current (DC) method using a current flow of 100 mA between the terminal Pt electrodes. For Seebeck coefficient measurements, a constant 30 K temperature difference was applied across the edges of the sample whilst the voltage and temperature differences were recorded between the two side probes. Thermal diffusivity measurements were carried out over the temperature range 373 K ≤ T ≤ 573 K in steps of 50 K using an Anter Flashline 3000 instrument. Measurements were made on 2-mm-thick, 13-mm-diameter pellets. This instrument determines both the thermal diffusivity (α) and the heat capacity (C_p) of the sample, and the thermal conductivity (λ) is calculated from the relationship: $\lambda = \alpha C_p d$, where d is the sample density. For the determination of the heat capacity, side-by-side testing of a reference material, Pyroceram™ 9606, of known heat capacity was carried out.

Module Fabrication

A TE module formed by nine couples of *n*-type $Yb_{0.36}Co_4Sb_{12}$ and *p*-type $Ce_{0.8}Fe_3CoSb_{12}$ skutterudite thermoelements was fabricated. Each leg was cut from hot-pressed ingots at 1.7 mm × 1.7 mm cross-sectional area and 2.0 mm length dimensions. Two 16 mm × 13 mm alumina plates with attached Cu strips (fabricated by European Thermodynamics Ltd.) were used to provide the thermal and electrical contacts. The formation of the junctions between the thermoelements and the Cu strips was performed by using fluxless $Zn_{78}Al_{22}$ solder bars (ZNAL22NC, melting point 755 K) and its flux paste

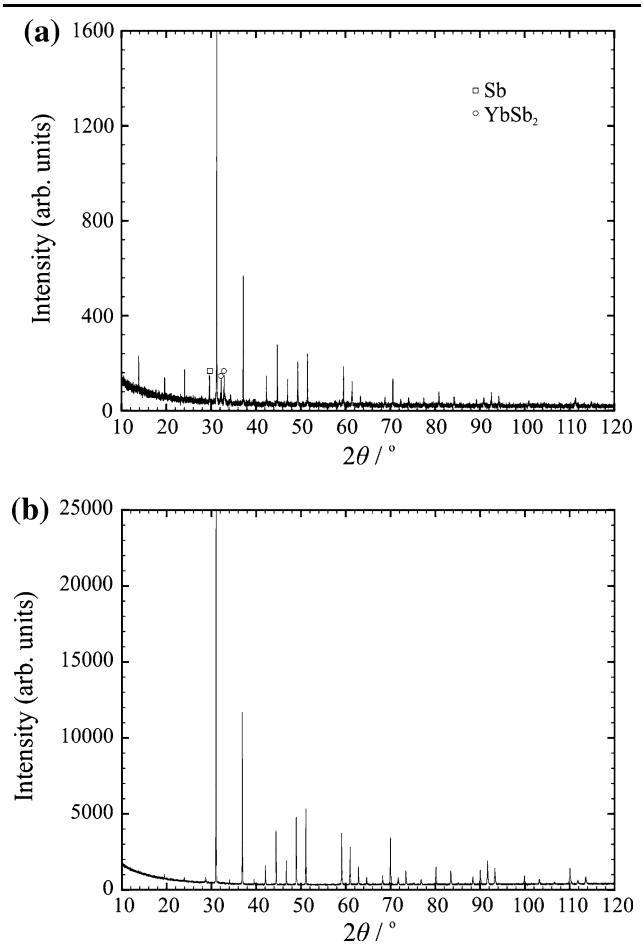

Fig. 1. Powder x-ray diffraction patterns for (a) $Yb_{0.36}Co_4Sb_{12}$ with a = 9.0460(3) Å and (b) $Ce_{0.8}Fe_3CoSb_{12}$ with a = 9.1127(1) Å.

(ZNALFLNC) purchased from Harris Products Group. Small pieces of solder bars were pressed and then cut to an area similar to the cross-sectional area of the thermoelement. Pd plating was performed onto the thermoelement parts to be joined using a plating pen (Hunter Products Inc.). All the components (i.e., thermoelements, alumina plates, and solder pieces) were sandwiched using a homemade assembly kit made out of stainless steel. To achieve a good soldered joint, flux paste was spread between both Pd-plated thermoelement/solder and solder/Cu strip interfaces. Once assembled, the setup was introduced into a quartz tube furnace, evacuated to ca. 4×10^{-2} torr, and heat-treated at 953 K for 10 min. After this time, the samples were extracted from the interior of the furnace and allowed to cool down to room temperature under vacuum. Finally, two contacting wires were soldered to the device to provide the contacts.

To evaluate the performance of the fabricated module, it was sandwiched between two Cu blocks, one of them with embedded cold water recirculation, which provided the cold side, and the other one with two heaters inserted, acting as the hot side. The temperature difference was measured with two K-type thermocouples located close to the ceramic plates. The power output was calculated in air at several temperature differences, maintaining the cold-side temperature around 293 K while gradually increasing the hot-side temperature up to 665 K. The internal module resistance (R_{in}) was calculated from the slope of the current–voltage plots obtained by connecting the module to a variable external load, whose resistance (R_L) was swept under constant temperature differences. The voltage at the load (V_L) was measured, and the current was calculated as $I = V_L/R_L$. After the measurement at the highest hot temperature, the heaters were switched off and the module was allowed to cool down to room temperature at its natural cooling rate. Finally, thermocycling experiments were carried out in air by increasing the hot-side temperature from room temperature up to 573 K while keeping the cold side at 293 K. This temperature difference was maintained while the current–voltage characteristics were measured and then allowed to dissipate. The device was cycled seven times.

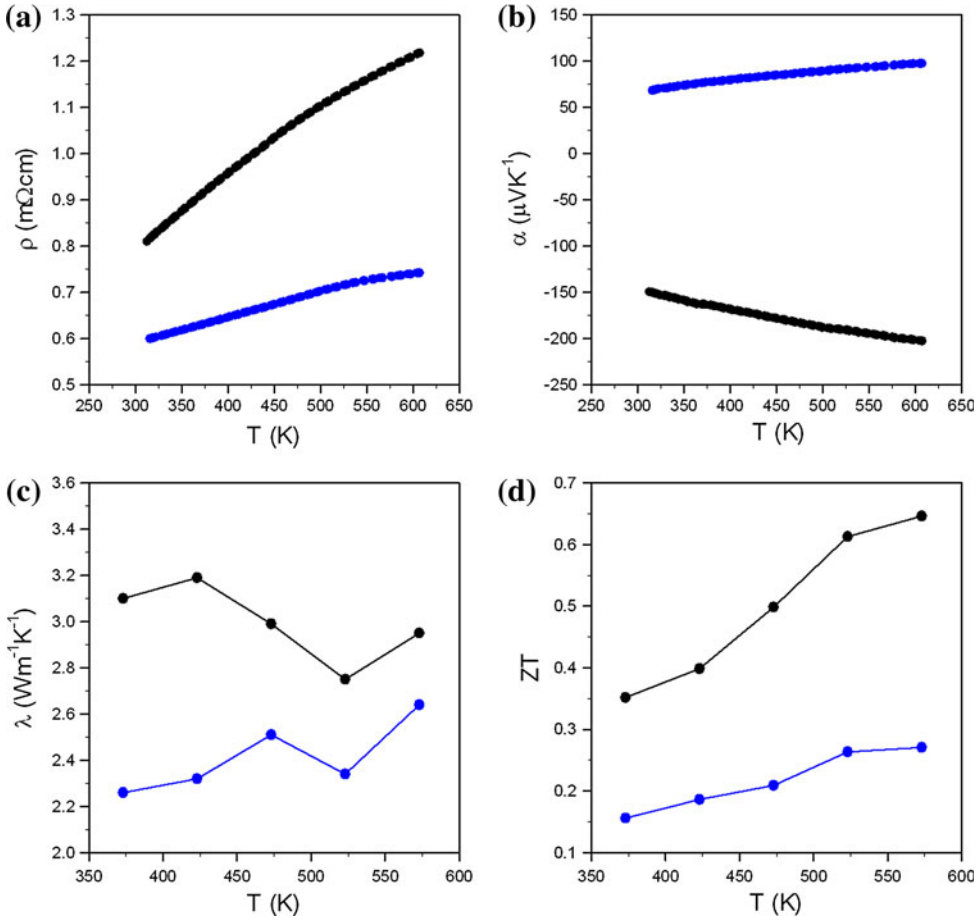

Fig. 2. (a) Electrical resistivity, (b) Seebeck coefficient, (c) thermal conductivity, and (d) *ZT* for *n*-type $Yb_{0.36}Co_4Sb_{12}$ (black) and *p*-type $Ce_{0.8}Fe_3CoSb_{12}$ (blue) as a function of temperature (Color figure online).

RESULTS

Materials Characterization and Physical Properties

The diffraction patterns (Fig. 1) of reaction products show that $Ce_{0.8}Fe_3CoSb_{12}$ contains no secondary phase whereas $Yb_{0.36}Co_4Sb_{12}$ contains small amounts of Sb and $YbSb_2$ impurities. Rietveld refinements were performed using the cubic space group $Im\ \bar{3}$, in which the filler sites are partially occupied with Ce or Yb atoms.

Figure 2 shows the physical properties for both *n*- and *p*-type skutterudites. The results are in accord with previously reported literature values for $Yb_xCo_4Sb_{12}$[12,13] and $Ce_xFe_3CoSb_{12}$.[14]

Module Evaluation

The methodology used for module fabrication has been proved to be valid for skutterudite-based devices. Optimizing the working conditions is a key task in the fabrication method, since small changes in time and temperature of the heating process, mismatches in the length of the thermoelements, unsuitable alignment, uneven pressures applied in the assembly, and the area and thickness of the solder pieces are different factors that can significantly influence the performance of the resulting device. Identifying the proper solder and metal barrier to be used is also crucial and dramatically affects the quality of the junctions. In our device, Pd plating onto the skutterudites has been employed after testing other metals such as Ag, Ni, and Cr that led to poorer junctions. Additionally, the atmosphere during the heating process is another key factor. Vacuum eliminates the presence of O_2, improving the soldering but also favoring sublimation of Sb from the skutterudites. Alternatively, Ar or N_2 atmospheres can also be used. These considerations show that there is a wide range of factors to optimize in order to achieve the best conditions for device fabrication.

The fabricated module and its output performance are shown in Fig. 3. It can be seen that higher power outputs can be obtained under larger temperature differences and that the module can be operated up to at least 660 K. Under a temperature difference of 365 K, the module is able to provide 157.4 mW power output. An internal module resistance of $R_{in} \approx 0.7\ \Omega$ was obtained and did not show a significant increase at higher temperatures, but did show a small decrease in the medium temperature range. If we subtract the contribution of materials, using the values shown in Fig. 2, from R_{in}, we can estimate an average specific contact resistivity value at room temperature of $4.77 \times 10^{-4}\ \Omega\ cm^2$, an order of magnitude above the preferred range of $10^{-5}\ \Omega\ cm^2$ to $10^{-7}\ \Omega\ cm^2$. The sources of this high contact resistance need to be further investigated in detail.

To compare the power generation of the module with other reported values, the volume power density

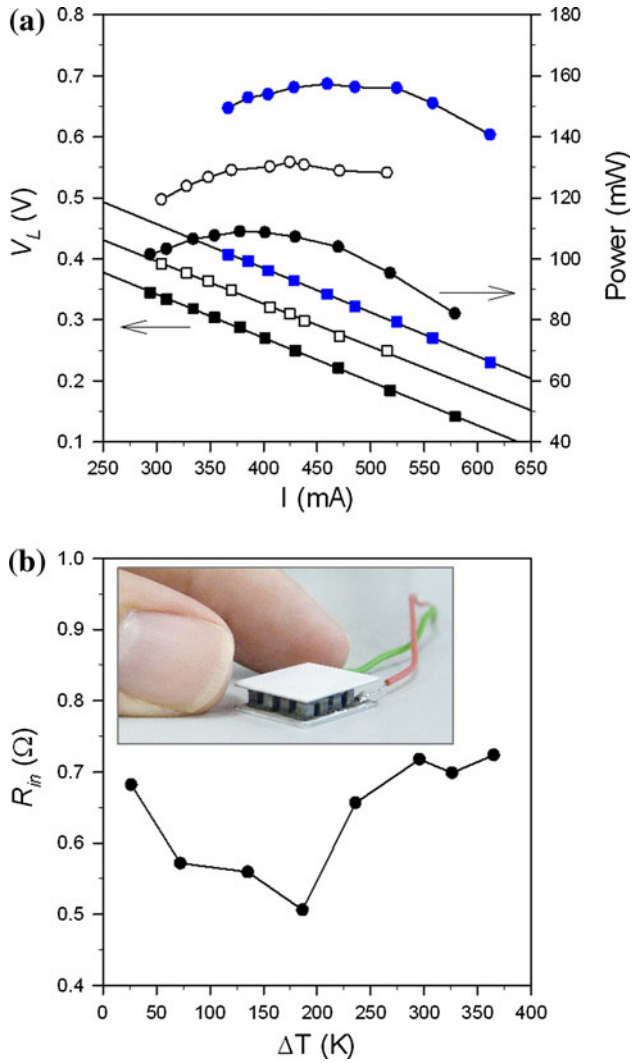

Fig. 3. (a) Power output (dots) and voltage at the load (squares) of the TE module at several temperature differences: 296 K (black), 326 K (white), and 365 K (blue). (b) Internal module resistance variation with temperature difference. The inset shows a picture of the fabricated module (Color figure online).

was calculated (Fig. 4). The values obtained are close to that of a previous skutterudite module fabricated by Matsubara.[15] Much higher power density is obtained when compared with a Bi_2Te_3/PbTe cascade module by Hori and Kusano,[16] a Mg_2Si module by Nemoto et al.,[17] and some oxide-based modules.[18,19]

To evaluate its high-temperature durability, the device was subjected to a thermocycling test. Figure 5 shows the variation of the open-circuit voltage (measured at zero current) and the internal module resistance with the number of cycles. Both properties show a variation from their initial (cycle 0) values on cycling. Since the R_{in} value after the last measurement at 365 K temperature difference during the initial characterization was similar to the fresh value of $R_{in} \approx 0.7\ \Omega$ (Fig. 3b), and the value measured in the first cycle was significantly higher (1.81 Ω), damage to the device was produced during

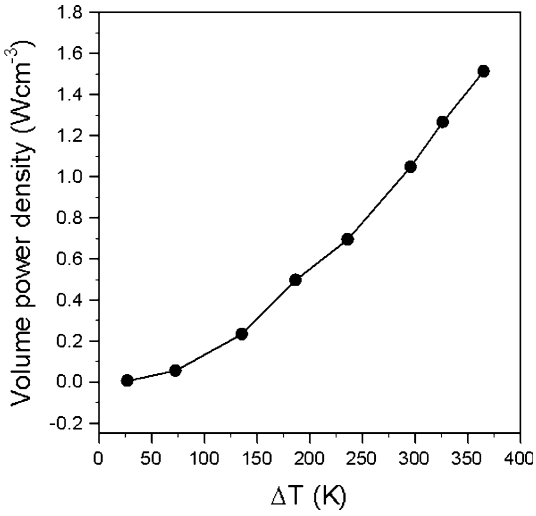

Fig. 4. Power output per TE materials volume versus temperature difference for the fabricated skutterudite module.

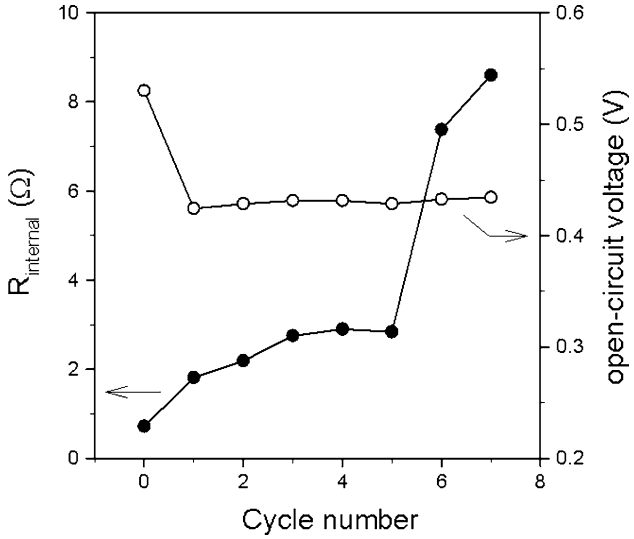

Fig. 5. Internal resistance (black) and open-circuit voltage (white) of the fabricated module versus the number of cycles performed at 280 K temperature difference. Cold-side temperature was kept at a constant value of 293 K. The initial internal module resistance and open-circuit values are plotted as cycle 0 and are the values found after collecting the data in Fig. 3.

the rapid cooling down from 660 K. Furthermore, R_{in} continues to increase and even reaches values higher than 7 Ω after the fifth cycle. On the contrary, the open-circuit voltage maintains a constant trend along all the cycles. This means that the main factor responsible for the increase in R_{in} is the contact resistance. The initial drop of the open-circuit voltage may be due to materials degradation undergone at the highest hot-side temperatures reached during the initial characterization. In fact, it is well known that $Yb_xCo_4Sb_{12}$ and $Ce_xFe_3CoSb_{12}$ begin to oxidize in air at 500 K and 650 K, respectively.[20,21] This reflects the need to protect or coat the skutterudites when operated in air.[22–24]

CONCLUSIONS

A simple methodology for fabrication of high-temperature TE devices has been described. It uses standard facilities and commercial products, which makes it easy to adapt to any laboratory. A skutterudite-based TE module was fabricated with this procedure, showing an output volume power density higher than 1.5 W cm^{-3} under 365 K temperature difference and an internal resistance and specific contact resistivity of 0.7 Ω and 4.77×10^{-4} Ω cm^2, respectively. The device showed performance degradation when operated at higher than 600 K hot-side temperature, attributed to materials oxidation in air. During thermocycling, the internal module resistance was significantly affected due to damage in the contacts. This research is an initial step toward proving the capability of the methodology. Significant further work is in progress to improve the final devices. Different commercial solders, chemical compatibilities with materials, temperature and time of heat treatment, and the vacuum level or different inert atmospheres are some of the parameters that can be optimized for improvement.

ACKNOWLEDGEMENTS

We thank the UK Engineering and Physical Sciences Research Council for financial support (EP/H050396).

REFERENCES

1. T.M. Tritt, D.R. Clarke, and P. Fratzl, *Ann. Rev. Mater. Res.* 41, 433 (2011).
2. J.R. Sootsman, D.Y. Chung, and M.G. Kanatzidis, *Angew. Chem. Int. Ed.* 48, 8616 (2009).
3. M. Zebarjadi, K. Esfarjani, M.S. Dresselhaus, Z.F. Ren, and G. Chen, *Energy Environ. Sci.* 5, 5147 (2012).
4. J. García-Cañadas and G. Min, *AIP Conf. Proc.* 1449, 454 (2012).
5. K.T. Wojciechowski, R. Zybala, and R. Mania, *Microelectron. Reliab.* 51, 1198 (2011).
6. J.Q. Guo, H.Y. Geng, T. Ochi, S. Suzuki, M. Kikuchi, Y. Yamaguchi, and S. Ito, *J. Electron. Mater.* 41, 1036 (2012).
7. D.G. Zhao, C.W. Tian, S.Q. Tang, Y.T. Liu, L.K. Jiang, and L.D. Chen, *Mater. Sci. Semicond. Process.* 13, 221 (2010).
8. K. Arai, M. Matsubara, Y. Sawada, T. Sakamoto, T. Kineri, Y. Kogo, T. Iida, and K. Nishio, *J. Electron. Mater.* 41, 1771 (2012).
9. T. Caillat, J.P. Fleurial, G.J. Snyder, A. Zoltan, D. Zoltan, and A. Borshchevsky, *XVIII International Conference on Thermoelectrics* (Baltimore, 1999).
10. M. Brignone and A. Ziggiotti, *AIP Conf. Proc.* 1449, 493 (2011).
11. A.C. Larson and R.B. von Dreele, *General Structure Analysis System* (Los Alamos Laboratory, Report LAUR 85-748, 1994).
12. G.S. Nolas, M. Kaeser, R.T. Littleton, and T.M. Tritt, *Appl. Phys. Lett.* 77, 1855 (2000).
13. H. Li, X. Tang, Q. Zhang, and C. Uher, *Appl. Phys. Lett.* 93, 252109 (2008).
14. B.C. Sales, D. Mandrus, B.C. Chakoumakos, V. Keppens, and J.R. Thompson, *Phys. Rev. B* 56, 15081 (1997).
15. K. Matsubara, *21st International Conference on Thermoelectrics* (Long Beach, 2002), p. 418.

16. Y. Hori and D. Kusano, *22nd International Conference on Thermoelectrics* (La Grande Motte, 2003), p. 602.
17. T. Nemoto, T. Iida, J. Sato, T. Sakamoto, T. Nakajima, and Y. Takanashi, *J. Electron. Mater.* 41, 1312 (2012).
18. H.M. Su, Y. Jiang, X.Z. Lan, X.M. Liu, H.H. Zhong, and D.B. Yu, *Phys. Status Solidi A* 208, 147 (2011).
19. A. Inagoya, D. Sawaki, Y. Horiuchi, S. Urata, R. Funahashi, and I. Terasaki, *J. Appl. Phys.* 110, 123712 (2011).
20. E. Godlewska, K. Zawadzka, A. Adamczyk, M. Mitoraj, and K. Mars, *Oxid. Met.* 74, 113 (2010).
21. A.V. Powell, A. Kaltzoglou, P. Vaqueiro, G. Min, J. Garcia-Cañadas, R.K. Stobart, J. Li, G. Dong, and A. Wijewardane, *AIP Conf. Proc.* 1449, 505 (2012).
22. M.S. El-Genk, H.H. Saber, T. Caillat, and J. Sakamoto, *Energy Convers. Manag.* 47, 174 (2006).
23. K. Zawadzka, E. Godlewska, K. Mars, and M. Nocun, *AIP Conf. Proc.* 1449, 231 (2011).
24. H.L. Dong, X.Y. Li, Y.S. Tang, J. Zou, X.Y. Huang, Y.F. Zhou, W. Jiang, G.J. Zhang, and L.D. Chen, *J. Alloys Compd.* 527, 247 (2012).